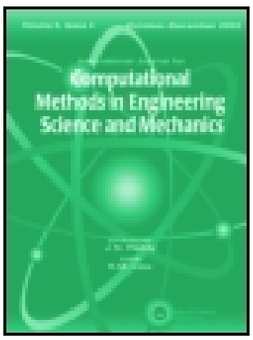

International Journal for Computational Methods in Engineering Science and Mechanics

ISSN: 1550-2287 (Print) 1550-2295 (Online) Journal homepage: http://www.tandfonline.com/loi/ucme20

Passive Mechanical Properties of Ovine Rumen Tissue

Stephen J Waite, John E Cater, Cameron G Walker, Satya Amirapu, Garry C Waghorn & Vinod Suresh

To cite this article: Stephen J Waite, John E Cater, Cameron G Walker, Satya Amirapu, Garry C Waghorn & Vinod Suresh (2016): Passive Mechanical Properties of Ovine Rumen Tissue, International Journal for Computational Methods in Engineering Science and Mechanics, DOI: 10.1080/15502287.2015.1082676

To link to this article: http://dx.doi.org/10.1080/15502287.2015.1082676

Accepted author version posted online: 17 May 2016.
Published online: 17 May 2016.

Passive Mechanical Properties of Ovine Rumen Tissue

Stephen J Waite[1*], John E Cater[2], Cameron G Walker[2], Satya Amirapu[3], Garry C Waghorn[4], Vinod Suresh[1,2]

1 Auckland Bioengineering Institute, University of Auckland, Auckland, New Zealand.

2 Department of Engineering Science, University of Auckland, Auckland, New Zealand.

3 Department of Anatomy with Radiology, University of Auckland, Auckland, New Zealand.

4 DairyNZ, Hamilton, New Zealand.

Abstract

Mechanical and structural properties of ovine rumen tissue have been determined using uniaxial tensile testing of tissue from four animals at five rumen locations and two orientations. Animal and orientation did not have a significant effect on the stress-strain response, but there was a significant difference between rumen locations. Histological studies showed two orthogonal muscle layers in all regions except the reticulum, which has a more isotropic structure. A quasi-linear viscoelastic model was fitted to the relaxation stage for each region. Model predictions of the ramp stage had RMS errors of 13%-24% and were within the range of the experimental data.

1 Introduction

The rumen is the first and largest compartment in the digestive tract in ruminant herbivores such as sheep and cows. Ingested feed is stored in the rumen and mixed by muscular contractions while undergoing digestion by microbial action. It is a large multi-compartmental organ divided by a series of folds and pillars into broadly five chambers as shown in (Figure 1) [Sellers and Stevens, 1966]. The dorsal and ventral sacs are the largest chambers and contribute the majority of the rumen volume. The dorsal and ventral blind sacs are located at the posterior end of the organ. The most anterior chamber is the reticulum which is separated from and communicates with the rest of the rumen by the ruminoreticular fold. A series of muscular bands of tissue or pillars define the outlines of the chambers. The rumen is lined by a layer of projecting papillae that varies in thickness across the different chambers and provides a large mucosal surface area for absorbing the products of digestion.

The microbiology and metabolism of the rumen have been extensively studied [Hungate, 1966] and [Baldwin, 1995] and has led to the development of mechanistic, predictive models of rumen digestion [Offner and Sauvant, 2004]. A similar quantitative understanding of rumen motility is currently lacking. Propulsive movements of the stomach were first explored in the late 1800s [Lewis, 1960] but with no means to record the movement little progress could be made. In the 1920s the principal rumen contractions and their sequence were observed via fistula observations, palpation and pressure measurements [Schalk and Amadon, 1928]. Measurement of wall motion and displacements using radiography [Wyburn, 1980] and [Akester and Titchen, 1969] and manometric measurements [Waghorn and Reid, 1984] have provided a better understanding of the magnitude of compartmental contractions. However, these studies have not provided a quantitative understanding of how motility affects mixing, particle dynamics and outflow in the rumen. The problem is particularly challenging due to the difficulty of making flow measurements in the con-

tracting rumen. One solution to this problem is to use computational modelling to represent the contracting boundaries of the rumen wall that drive digestive flow within a computational fluid dynamics (CFD) environment. This model could then be used to analyse the effects of feed type, its particle size and decomposition rate, on the mixing and outflow of the digestive contents through the rumen. Such an understanding would be useful in explaining observations that have linked methane emissions from ruminants with feed intake [Hammond et al., 2013], rumen outflow rates [Pinares-Patino et al., 2011] and rumen volume [Bain et al., 2014]. This paper presents the results of an investigation into the mechanical and structural properties of rumen tissue which can be used to formulate such a model.

2 Materials and Methods

Material Collection

Rumens were obtained from four healthy, pregnant ewes aged 4-5 years that were killed as part of another study approved by the Animal Ethics Committee of the University of Auckland. Gastrointestinal tissues from the carcasses were made available to us after the removal of the fetuses as part of the institution's commitment to the 3R principles of reduction, refinement and replacement for the use of animals in research.

Sample Preparation

The rumen was disconnected from the esophagus and omasum, emptied, rinsed with water and then refrigerated in a phosphate buffered saline (PBS) solution. The organ was then dissected into five sections; the reticulum, ventral sac, dorsal sac, caudo-ventral blind sac and the caudo-dorsal blind sac (Figure 1(a)). These sections were washed with water to remove digestive contents from the papillae layer as well as blood and interstitial fluid. The sections were then stored in fresh PBS

solution and refrigerated for 48 hours before testing.

Strain Analysis

A natural striation pattern was visible on the surface of the rumen tissue (Figure 1b) that likely reflects structural organisation in the underlying tissue. Therefore, samples were cut parallel and perpendicular to this surface feature to assess the effects of tissue anisotropy on mechanical properties. Three samples were taken from each region for each orientation resulting in a total of 120 samples. Samples were cut from the tissue with a custom-fabricated tool comprising of razor blades held into shape by acrylic sections. This tool was used to stencil cut the tissue before a surgical scalpel was used to completely separate the sample section from the surrounding tissue (Figure 2a). This minimised sample shape distortions and provided consistent dimensions of the test section for all samples. The test section was rectangular with a width of 5 mm and length of 20 mm. The length was chosen to be 4 widths long to satisfy Saint-Venant's principle to achieve a uniform stress state within the centre of the gauge. The clamped sections of the sample have a width of 15 mm to increase the contact area to help prevent slippage from the clamps. The thickness of each sample was measured using vernier calipers at three locations along the gauge. The mean thicknesses for each location and animal were found to be approximately constant (Table 1).

Testing Protocol

The uniaxial force-displacement response and relaxation of the tissue was measured using an Instron 5866 Series tensometer with a 2.5N load cell. The clamps were custom made from 6 mm thick acrylic sheets and lined with abrasive paper to prevent slippage. Refrigerated samples were allowed to warm to room temperature before being clamped into place. Samples were secured in clamps under the following conditions. The distance between the two clamp ends was set as 20mm, the gauge length of the samples. The sample was then secured into the top clamp and allowed to

hang freely into the lower clamp under its own weight before the lower clamp was secured. In the majority of cases satisfactory alignment between the sample and the lower clamp was achieved without the need for further manipulation. In a few cases when there was some shrinkage or curling of the sample after it was removed from surrounding tissue, samples were gently uncurled into the lower clamp using tweezers. A small force preload of 0.1N was then applied to remove any slack and define a zero strain position. Samples were preconditioned for ten cycles to a strain of 20% at a rate of 0.2 mm/second to achieve a repeatable stress state. Samples then underwent a tensile ramp to 40% strain at a rate of 0.2 mm/second and were then held for 90 seconds at this extension to capture stress relaxation within the tissue.

Data and Statistical Analysis

Stress is calculated as the measured force F, divided by the cross sectional area A. As the induced strain of the sample is large, (40%), the cross sectional area cannot be assumed to be constant. The tissue was assumed to be incompressible [Chen et al., 1996] and so stress was defined as,

$$\sigma = \frac{F}{A_0}(\epsilon + 1), \tag{1}$$

where ϵ is the engineering strain, and A_0 is the cross sectional area of the sample in the unstrained state. For the statistical analysis, stress from each experiment was sampled at four time points corresponding to low strain $\epsilon(t = 20s) = 20\%$, peak stain $\epsilon(t = 40s) = 40\%$, early relaxation $t = 50s$ and late relaxation $t = 120s$. A repeated measures model was fitted with fixed effects to explain the sample stress in terms of the animal, orientation, region and time. Interaction terms were considered for region & time, orientation & time and region & orientation. Initial analysis indicated that the interaction term for region & orientation was not significant, and so it was removed from the model. Animal was also not significant, but was kept in the model to allow for any possible confounding due to this variable. A correlation structure was also included, to capture the correlation between repeated measurements in the same sample. We considered compound

symmetry, first order autoregressive (AR(1)), Toeplitz and unstructured models. The unstructured model was deemed to have too many variables given the amount of data and was discarded to avoid over-fitting. The Toeplitz model was preferred based on the outcome of the likelihood ratio test. All analysis was conducted using SAS 9.4 [*SAS* Institute Inc., 2013]. Correlations with $P < 0.05$ are assumed to be significant.

Histology

Tissue samples were taken from each of the five locations, as shown in Figure 1, from two of the rumens, totaling ten samples. They were then fixed in 10% neutral buffered formalin. Samples were transferred into cassettes and dehydrated through a series of graded ethanol baths and infiltrated with wax in a Leica APS300S autoprocessor. The infiltrated tissues were then embedded into paraffin wax blocks at a Leica embedding centre. The wax blocks were cut at $5\mu m$ on a Leica Microtome RM2245 and picked up onto Superfrost Plus adhesive slides. Slides were dried at $60^{\circ}C$ using a Contherm oven. The paraffin sections were deparaffinised and hydrated in water. Masson's trichrome staining was performed and slides were imaged to visualise tissue structure and the distribution of smooth muscle and collagen.

3 Mathematical Modelling

To capture the non-linear stress-strain characteristics of the rumen tissue, a quasi-linear viscoelastic model [Fung, 1981] was used to quantify the time-dependent mechanical properties. According to this model the stress σ at time t is given by the convolution integral of a reduced relaxation factor G and a strain (ϵ) dependent on elastic response σ^e,

$$\sigma(t) = \int_{-\infty}^{t} G(t-\tau)\frac{\partial \sigma^e(\epsilon(t))}{\partial \epsilon}\frac{\partial \epsilon}{\partial \tau}d\tau. \tag{2}$$

The reduced relaxation function is described by Fung to take the form,

$$G(t) = \left\{1 + c\left[E_1\left(\frac{t}{\tau_2}\right) - E_1\left(\frac{t}{\tau_1}\right)\right]\right\}\left[1 + c\ \ln\left(\frac{\tau_2}{\tau_1}\right)\right]^{-1}, \tag{3}$$

where $E_1(z)$ is the exponential integral,

$$E_1(z) = \int_z^\infty \frac{e^{-t}}{t} dt, \tag{4}$$

and c, τ_1, τ_2 are material constants. The elastic response was expressed by a rising exponential [Woo et al., 1981],

$$\sigma^e(\epsilon) = A(e^{B\epsilon} - 1). \tag{5}$$

The coefficients τ_1, τ_2, c, A and B were determined by fitting to the experimental data. The samples undergo a linear ramp extension until time t_0. This period is followed by a hold at constant strain to capture relaxation. The strain rate is therefore defined as,

$$\frac{\partial \epsilon(t)}{\partial t} = \begin{cases} \gamma & \text{if } t \leq t_0 \\ 0 & \text{if } t > t_0. \end{cases} \tag{6}$$

The material parameters were fitted only to the relaxation data from the 90 second hold period to evaluate the predictive capabilities of the model against the ramping phase [Nekouzadeh et al., 2007]. The parameters were fitted using the MATLAB [The MathWorks Inc., 2013] function fminunc() that performs unconstrained nonlinear optimization. The initial guess for the algorithm was chosen to approximate the experimental values of the peak stress at $t = 40s$ and the initial curvature of the relaxation phase. Preliminary studies showed that allowing the initial guess to under-predict the relaxation curve resulted in a poor fit to the early stages ($t < 45s$) of relaxation. The initial guess was therefore chosen to slightly over predict the data. The data was also sub-sampled to give more weighting to the early relaxation period, in order to provide a more uniform spread of error over the whole curve. 1000 data points were sampled over the test period, between 0 and 130 seconds. To sub-sample the data, every 5th data point was taken for values ranging

between 40 and 45 seconds, the region where the majority of stress relaxation occurred. Every 10th data point was taken from time values greater then 45 seconds. These values were selected based on visual inspection of the fitted curve to the relaxation data. The fitted parameters were then used to predict the loading ramp. The root mean squared (RMS) error between experimental points and the fitted model is given by

$$error = \sqrt{\frac{\sum_{n=0}^{n=N} \left(\frac{\sigma_{fit}(n) - \sigma_{exp}(n)}{\sigma_{exp}(n)}\right)^2}{N}}. \quad (7)$$

4 Results

Figure 3 shows the mean stress against time for each location and orientation for all four rumens. At small strains (<20%, $t < 20s$), the rumen tissue is compliant and develops very little stress in response to deformation. At larger strains (20%< ϵ <40%, $20s < t < 40s$) the tissue stiffens significantly for all locations with the exception of the ventral blind sac in the parallel orientation, which exhibts a much more gradual increase in stress. A significant degree of stress relaxation was observed in all samples with the peak stress decreasing between 24% and 53%. The plots also show considerable variation between certain regions of the rumen and orientations of the samples.

The statistical analysis indicated that the effects of animal and the interaction between orientation & region were not significant ($P = 0.28$ and $P = 0.56$ respectively), while region, time, orientation and the interaction of region & time and orientation & time are all significant ($P < .0001$). At strains up to 20% ($t \leq 20s$), there was no significant difference between any of the five regions. At the peak strain (40%, $t = 40s$), significant differences were found between some of the different regions (Table 2). The dorsal sac is significantly stiffer from all other regions, achieving a peak stress of 61 kPa at peak strain. Similarly, the ventral sac is also significantly less stiff than the dorsal blind sac and ventral blind sac, with a peak stress of 22 kPa. There is no significant difference between that dorsal blind sac, ventral blind sac and reticulum, which achieved peak stresses of 38

kPa, 44 kPa and 32 kPa respectively.

Since the statistical analysis indicated no significant difference between animals, the QLV model was fitted to the mean of all animals for each region and orientation. Fitted parameter values are listed in Tables 3 and 4. The model provides an excellent fit to the relaxation phase with RMS errors of <2%. Model predictions of the loading ramp have RMS errors of 13%-24%. Figure 4 indicates that the model tends to under-predict the true stress.

The ventral sac, which had RMS errors of 17.4% and 18.6% when used to predict the ramp stages for parallel and perpendicular orientations respectively, represents the trend observed for low RMS error or a good fit to the model (Figure 4(d)). The error is spread across the entire ramp period, with the curve under-predicting the stress response. In contrast, the ventral blind sac represents a poor fit with RMS errors of 23.1% and 23.5%. The model under-predicts the stress response at the later strain period, $20s < t < 40s$, and over-predicts during the initial strain ($t < 20s$). Tables 3 and 4 present the fitted material parameters for each model as well as the RMS error for the fitted relaxation curve and predicted ramp curve for parallel and perpendicular orientations. For both orientations, the ventral blind sac has the poorest results when predicting the ramp curve. In both orientations there is also a significant and rapid change in the gradient of the initial strain range. The reticulum data has the best fit for both orientations.

While the statistical model indicated that there was no significant difference for the effect of interaction between orientation & region, we observe a distinct pattern in the aggregated data for all five locations, whereby the perpendicular samples develop a stress that is at least as high as the parallel samples. This observation is only qualitative and a larger sample size is required to demonstrate a significant effect of sample orientation on the stress response.

Figure 5 shows the ultra-structural features of rumen tissue at different locations visualised by Massons trichrome stain. A darkly stained epithelial layer lines the rumen and papillae on the mucosal surface at the right of the images. Underneath the epithelium is a thin layer of smooth mus-

cle (pink) that is supported by a connective tissue layer interspersed with collagen fibres (green). This is followed by two distinct layers of smooth muscle oriented orthogonally to each other that correspond to the longitudinal and circular layers observed in the gastrointestinal tracts of other mammals including humans. While this basic arrangement is observed in all rumen locations (except the reticulum, see below), the samples in Figure 6 have been selected to illustrate structural differences that were observed between the locations. In the ventral sac (Figure 5a) and the ventral blind sac the two muscle layers are of comparable thickness, whereas in the dorsal sac (Figure 5b) and dorsal blind sac, the inner layer (closer to the mucosal surface) is much thicker than the outer layer. The reticulum (Figure 5c) shows a significantly different structure compared to the other four locations. There is not a distinctive layer of connective tissue within the muscle tissue, although there are thin bands of connective tissue spread throughout the muscle layer. Distinct muscle layers cannot be identified and the orientation of the muscle appears to vary spatially across the sample, giving rise to a more isotropic structure.

5 Discussion and Conclusions

We have carried out the first characterisation of the mechanical and structural properties of the sheep rumen and their spatial variation. Adjacent samples from the same rumen region as well as samples from different regions showed large variability in stress during uniaxial extension (Figure 3). The variability could result from variations in the experimental procedure or could reflect the inherent spatial variation in the tissue. Sample preparation procedures were standardised and carefully executed to minimise variability arising from differences in shape, gauge length, temperature and age of the tissue. An additional confounding factor could be the measurement of sample thickness which was made difficult by the variable height of the papillae. Errors in estimating the true tissue thickness would affect the cross sectional area and hence the calculated stress. We believe that this was not a significant factor for two reasons. First, the thickness measurements

at three locations for each sample were consistent. Second, the raw force data exhibited a similar level of variation as the calculated stress, suggesting that the calculation of the cross sectional area did not introduce additional variability. It is therefore likely that the variability reflects spatial inhomogeneity in tissue properties. This conclusion is supported by the statistical and histological analysis.

The statistical model indicated that there are significant differences in the stress values between different regions of the rumen to a high degree of confidence (Table 2). The dorsal sac was significantly stiffer than all other regions, which could be attributed to it being required to support the weight of the digestive contents. Similarly, the reticulum, dorsal blind sac, and ventral blind sac, which all undergo strong muscular contractions during digestion, were stiffer then the ventral sac. By contrast the ventral sac is left free hanging and while some movement of the ventral floor is reported in literature during contraction [Waghorn and Reid, 1984], it may not experience as intense contractions as the other regions during a contractive cycle.

Imaging of stained sections indicates visually striking differences in the organisation of muscle and collagen layers in different regions of the rumen (Figure 5). The statistical model indicated that the effect of interaction between tissue orientation & sample region did not have a significant effect on the measured stress. When the data from different animals were aggregated, measurements in the orientation perpendicular to the surface striations were found to be consistently higher than the parallel orientation for all locations excluding the reticulum (Figure 4). However, a relation between the surface structure and the underlying collagen and muscle fibre orientation is not known. Further analysis is required before the mechanical properties can be related to tissue composition.

All regions except the reticulum showed the presence of two distinct muscle layers oriented orthogonal to each other. In the reticulum the muscle layers were disorganised leading to a more isotropic appearance. Thus the true effect of orientation may be masked by the sample-to-sample variability and a larger sample size could place these qualitative observations on firmer ground.

As a first attempt to mathematically describe the mechanical properties of rumen tissue we fitted a QLV model to the relaxation data and used the fitted parameters to predict the extension. The predicted values were generally within the spread of the measurements. The model parameters offer some insight into the mechanical behaviour of the tissue. At small strains the elastic response component (Equation 5) is linear in strain and the product AB is equivalent to a Young's Modulus. This measure varies from 410 Pa to 1350 Pa between regions and orientations indicating a large degree of variation at small low strains. The stress at peak strain seems to be largely controlled by B since the most stiff (dorsal sac) and least stiff (ventral sac) regions have the largest and smallest values of this parameter. The time constants (τ_1 and τ_2) in the relaxation function represent the limits of the continuous spectrum in the QLV model. The wide range ($10^{-5}s$ to $10^{2}s$) indicates that rumen tissue components relax at very different time scales. The fraction of residual elastic stress after a long relaxation as $t \to \infty$ is given by,

$$E_R = \left[1 + c\ \ln\left(\frac{\tau_2}{\tau_1}\right)\right]^{-1} \tag{8}$$

,

which varies from 0.15 to 0.28 for the different regions and samples. A more complete constitutive model for rumen tissue would need to account for anisotropy and spatial variation in mechanical properties. Such a model would need to be based upon the stress profile that would be induced by a two-dimensional strain field. This will be the focus of future work.

Acknowledgements

We wish to acknowledge and thank Linley Nisbet for her technical assistance with procuring and dissection of rumen tissue. We would also like to thank Professor Laura Bennet and the Fetal Physiology and Neuroscience Group for making the animals used in the study available to us. Stephen Waite acknowledges financial support from the Auckland Bioengineering Institute for this study.

References

A.R. Akester and D.A. Titchen. Radiographic studies of the reticulo-rumen in the sheep. *Journal of Anatomy*, 104:137–152, 1969.

W.E. Bain, N.B. Bezuidenhout, L. andJopson, C Pinares-Patino, and J.C. McEwan. Rumen differences between sheep identified as being low or high methane emitters. *Proceedings, 10th World Congress of Genetics Applied to Livestock Production*, 2014.

R.L. Baldwin. *Modeling Ruminant Digestion and Metabolism*. Springer, 1995.

E.J. Chen, J. Novakofski, W.K. Jenkins, and W.D.Jr. O'Brien. Young's modulus measurements of soft tissues with application to elasticity imaging. *IEEE Transatcionts on ultrasonics,ferroelectrics, and frequency control*, 43:191–194, 1996.

Y.C. Fung. *Biomechanics: Mechanical Properties of Living Tissues*. Biomechanics. Springer New York, 1981. ISBN 9780387979472.

K.J. Hammond, J.L. Burke, J.P. Koolaard, S. Muetzel, C.S. Pinares-Patio, and G.C. Waghorn. Effects of feed intake on entric methane emissions from sheep fed fresh white clover (trifolium repens) and perennial ryegrass (lolium perenne) forgaes. *Animal Feed Science and Technology*, 179:121 – 132, 2013.

R.E. Hungate. *The rumen and its microbes*. Academic Press, 1966.

D. Lewis. *Digestive Physiology and Nutrition of the Ruminants: Proceedings of the University of Nottingham Seventh Easter School in Agricultural Sciences*. University of Nottingham Press, 1960.

A Nekouzadeh, K.M. Pryse, E.L. Elson, and G.M. Genin. A simplified approach to quasi-linear viscoelastic modeling. *Journal of Biomechanics*, 40:3070–3078, 2007.

A. Offner and D. Sauvant. Comparative evaluation of the Molly, CNCPS, and LES rumen models. *Animal Feed Science and Technology*, 112:107–130, 2004.

C.S. Pinares-Patino, S.H. Ebrahimi, J.C. McEwan, K.G. Dodds, H. Clark, and D. Luo. Is rumen retention

time implicated in sheep differences in methane emission? *New Zealand Society of Animal Production*, 71:219–222, 2011.

F.A. Schalk and R.S. Amadon. Physiology of the ruminant stomach (bovine): study of the dynamic factors. *Agricultural Experiment Station, North Dakota Agricultural College [Fargo]*, 216, 1928.

A.F. Sellers and C.E. Stevens. Motor fuctions of the ruminant forestomach. *Phsiological Reviews*, 46: 634–661, 1966.

SAS Institute Inc. *SAS/STAT Software, Version 9.4*. Cary, NC, 2013. URL `http://www.sas.com/`.

The MathWorks Inc. *MATLAB, version 8.2.0 (R2013b)*. Natick, Massachusetts, 2013. URL `http://www.mathworks.com/`.

G.C. Waghorn and G.S.W Reid. Resting level and vertical displacement of the cranial pillar and other structures in the ruminoreticulum of cattle of known bloat susceptibility. *New Zealand Journal of Agricultural Research*, 27:481–490, 1984.

S.L-Y. Woo, M.A. Gomez, and W.H. Akeson. The time and history-dependent viscoelastic properties of the canine medial collateral ligament. *Biomechanical Engineering*, 103:293–298, 1981.

R.S. Wyburn. The mixing and propulsion of the stomach contents of ruminants. *Digestive Physiology and Metabolism in Ruminants*, pages 35–51, 1980.

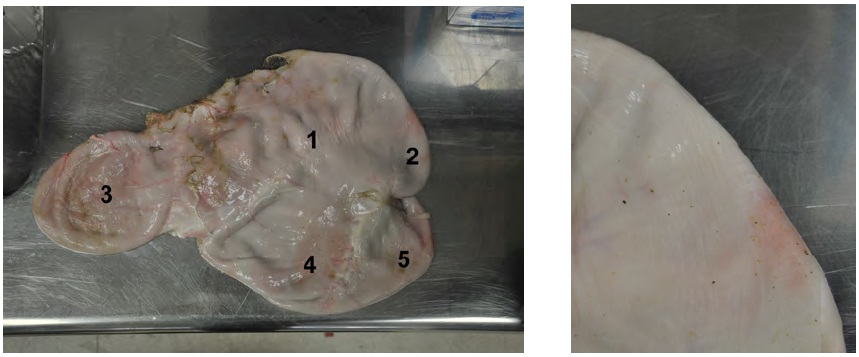

(a) (b)

Figure 1: (a) Intact sheep rumen showing the regions sampled for mechanical and histological testing. (1) dorsal sac, (2) dorsal blind sac (3) reticulum (4) ventral sac (5) ventral blind sac, (b) Example of striation patterns visible on the surface of the rumen.

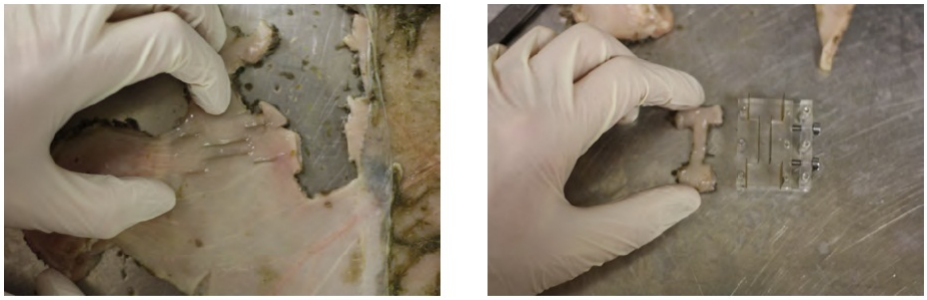

Figure 2: Sample preparation. (a) The tissue has been marked using the sample tool. (b) A surgical scalpel is then used to trace around the outside of the tissue and a repeatable sample is produced.

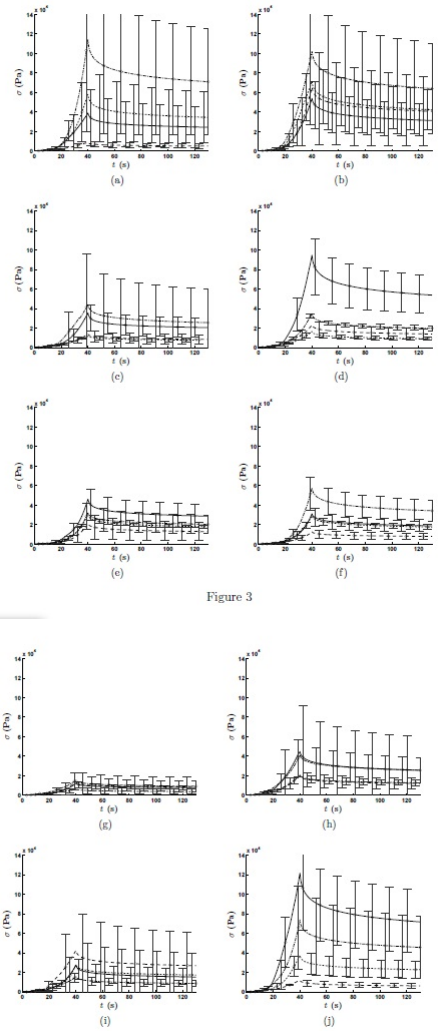

Figure 3

Figure 3: Location means and standard deviation for each rumen for parallel (left column) and perpendicular (right column) samples. (a-b) Dorsal sac, (c-d) dorsal blind sac, (e-f) reticulum, (g-h) ventral sac, (i-j) ventral blind sac.

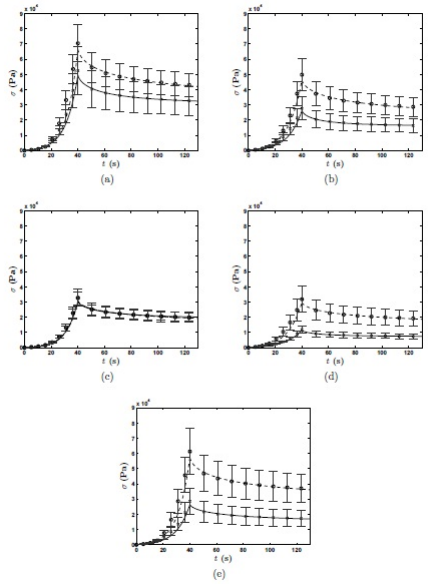

Figure 4: QLV models fitted to the population means (solid line for parallel, dashed line for perpendicular) compared to experimental values and standard error for both parallel (crosses) and perpendicular (circles) sample means. (a) Dorsal sac, (b) dorsal blind sac, (c) reticulum, (d) ventral sac, (e) ventral blind sac.

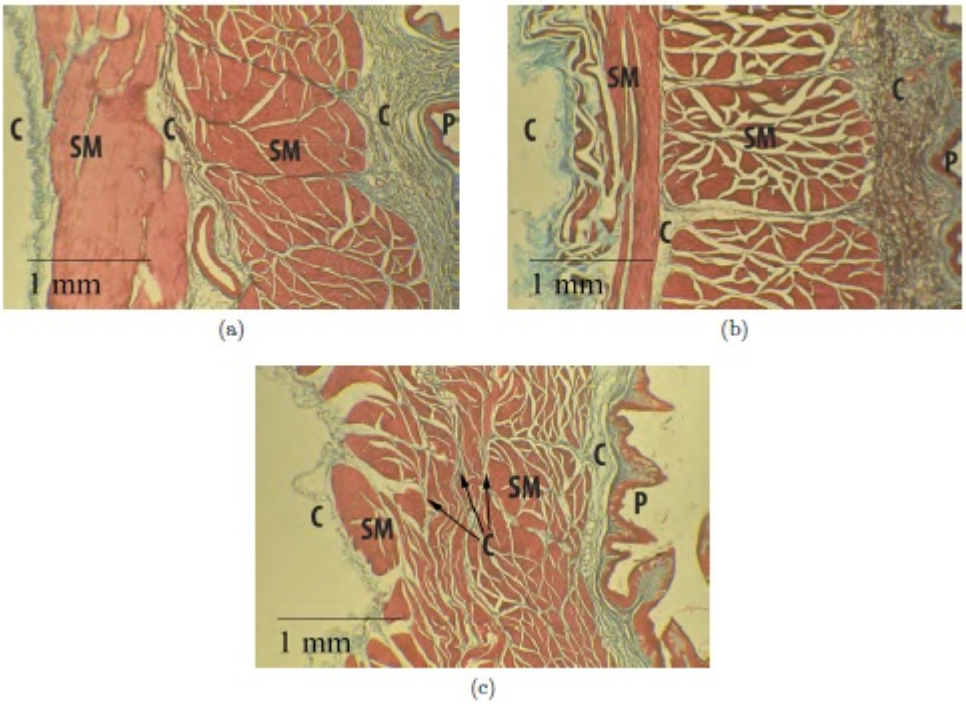

Figure 5: Histological samples for sections stained with Masson's Trichrome. (a) Ventral sac, (b) dorsal sac, (c) reticulum. SM=smooth muscle, C=collagen, P=papillae.

Table 1: Sample Thickness (mean ± standard deviation in mm, $n = 6$)

Location	Animal 1	Animal 2	Animal 3	Animal 4
Dorsal sac	3.76 ± 0.35	3.92 ± 0.31	2.82 ± 0.41	2.81 ± 0.4
Dorsal blind sac	3.58 ± 0.86	3.73 ± 0.56	3.32 ± 0.33	2.90 ± 0.15
Reticulum	3.37 ± 0.53	3.96 ± 0.54	3.87 ± 0.37	3.39 ± 0.27
Ventral sac	3.49 ± 0.27	3.54 ± 0.56	3.47 ± 0.12	2.97 ± 0.4
Ventral blind sac	3.00 ± 1.02	3.56 ± 0.56	2.77 ± 0.83	2.37 ± 0.56

Table 2: Significance Between Regions at $t = 40$.

Location	**DS**	**DBS**	**Retic**	**VS**	**VBS**
Dorsal Sac	–	0.0015	0.0001	< .0001	0.0246
Dorsal Blind Sac	0.0015	–	*n.s*	0.0226	*n.s*
Reticulum	0.0001	*n.s*	–	*n.s*	*n.s*
Ventral Sac	< .0001	0.0226	*n.s*	–	0.0029
Ventral Blind Sac	0.0246	*n.s*	*n.s*	0.0029	–

Table 3: Fitted Coefficients & Error for Fitted Parallel Location Means.

Location	A	B	C	τ_1	τ_2	ϵ_{ramp}	$\epsilon_{relaxation}$
Dorsal Sac	1700	0.56	0.24	8.0×10^{-6}	100	16.8%	0.6%
Dorsal Blind Sac	2000	0.49	0.34	2.3×10^{-5}	50	18.4%	0.9%
Reticulum	800	0.58	0.24	7.5×10^{-5}	102	13.4%	0.6%
Ventral Sac	1000	0.41	0.33	1.8×10^{-2}	50	17.4%	1.0%
Ventral Blind Sac	1400	0.51	0.26	8.5×10^{-6}	200	23.1%	1.2%

Table 4: Fitted Coefficients & Error for Fitted Perpendicular Location Means.

Location	A	B	C	τ_1	τ_2	ϵ_{ramp}	$\epsilon_{relaxation}$
Dorsal Sac	1200	0.63	0.27	4.8×10^{-6}	500	24.1%	1.0%
Dorsal Blind Sac	2700	0.50	0.33	3.2×10^{-5}	400	24.0%	1.4%
Reticulum	800	0.59	0.27	4.6×10^{-6}	400	16.7%	1.1%
Ventral Sac	2000	0.48	0.30	2.8×10^{-6}	500	18.6%	1.2%
Ventral Blind Sac	1800	0.57	0.26	4.9×10^{-6}	300	23.5%	1.2%